In-depth Analysis on Radiation Induced Multi-level Dark Current Random Telegraph Signal in Silicon Solid State Image Sensors

Clémentine Durnez, *Student Member, IEEE,* Vincent Goiffon, *Member, IEEE,*
Cédric Virmontois, *Member, IEEE,* Jean-Marc Belloir, *Student Member, IEEE,* Pierre Magnan, *Member, IEEE,*
and Laurent Rubaldo

***Abstract*—Radiation-induced phenomena constitute a big concern for image sensors dedicated to space application. Particles (such as protons or electrons) can impact the crystalline structure of the detector and create switches in the dark response. This may be a problem, especially for calibration and so on image quality. This article aims at expressing the method used for switch detection and showing some properties of these Random Telegraph Signals (RTS), concerning, among other things, their amplitudes, discrete levels, and switching times. A first analysis of these results is also given.**

***Index Terms*—Random Telegraph Signal, Radiation induced phenomenon, CMOS image sensor**

I. Introduction

HIGH-end image sensors are now able to detect very low flux because their parasitic dark current is increasingly low. However, the slightest fluctuation in this dark signal can lead to important consequences. Indeed, when exposed to radiations for example, image sensors are impacted by many particles which can cause displacement damage, moving atoms in the crystalline structure. They create permanent or temporary defects which can introduce energy levels in the bandgap of silicon. Some of these defects are known as Random Telegraph Signal (RTS) centers, and are a real trouble for calibration, because their dark signal switches randomly between two or more discrete states (see for example Sec. III-A for typical RTS signals). Several studies have already been conducted on CCD [1], [2] and CMOS image sensors [3], [4], but different hypotheses have been exposed about the origin of the phenomenon, and the cause is still not completely understood yet. The goal of this work is to present in-depth analysis of multi-level RTS signals, based on some new parameters extraction methods, in order to obtain the defect signatures and main RTS characteristics (the number of discrete levels, switching frequency, and amplitude between discrete levels).

C.Durnez, V.Goiffon, J-M.Belloir and P.Magnan are with ISAE-SUPAERO, Université de Toulouse, Image Sensor Research Team, Toulouse,France (e-mail: clementine.durnez@isae.fr).

C.Virmontois is with CNES (Centre National d'Études Spatiales), Toulouse, France.

L.Rubaldo is with SOFRADIR, Veurey-Voroize, France.

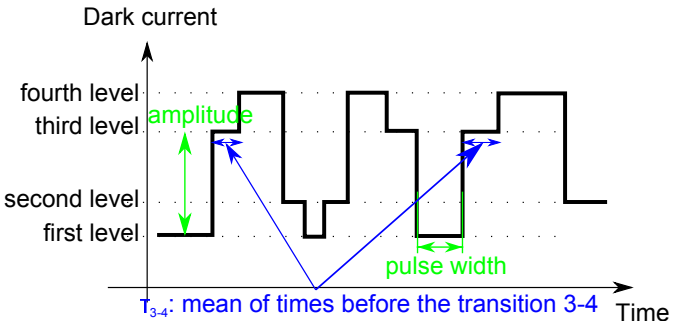

Fig. 1. Ideal RTS signal : there are four amplitudes (the transitions between the second and third level, and between the first and fourth level do not occur), one pulse width is shown, and two times contributing to the calculation of the time constant before the transition from third to fourth level are represented.

II. Pixels Detection and Algorithm Improvements

A. Definition of terms

First of all, DC-RTS (Dark Current RTS) can be defined as a switching leakage current [5]. If many dark images are acquired successively during a long time, pixels can blink from a gray level to another gray level with random switching time. This phenomenon has been observed in image sensors with CCD [1] and CMOS [4] technologies, and it has also been seen in other PN junctions such as in DRAM [6] or MOSFET [7]. In the literature, RTS is attributed to several causes such as oxide or bulk (depending on the incident particle) SRH generation centers [8] coupled or not with electric field enhancement [2], [4] or else modulation of a parasitic current [7]. Hence, it is important to extract most of typical RTS characteristics, in order to predict and mitigate this phenomenon to improve our understanding on this subject.

Fig. 1 illustrates the main parameters. As RTS centers are considered to be metastable generation centers, the discrete levels represent configurations in which the center is stable and has a given generation rate. Thus, if there is only one center in the pixel, the number of levels gives the number of visible configurations and amplitudes represent the differences between the generation rates of the center. A

link between levels and configurations will be developed in section III-C. The time between two transitions provides an information about the configuration stability. If a center is more stable in a given configuration, it will stay longer in that one.

In what follows, a pulse width will refer to a level width (i.e a time interval) between two transitions. The average time in a level will be defined as the mean time spent in a given level between two transitions and whatever the next transition. For example, a three-level RTS will have three distinct average times per level, and these times are actually the mean of all pulse widths which occur in each given level. On the contrary, a time constant will be the mean time spent in a given level, before a given transition. An example is given on Fig. 1, where the time constant τ_{3-4} represents the mean of times shown in blue, and stands for the time spent in third level before the transition which leads to the fourth one, whereas the average time in the third level corresponds to the time spent in this level whatever the next transition (the time in the third level before the transition to the first level is also taken into account).

Moreover, an amplitude will be defined as the height of a jump between two discrete levels. All amplitudes which actually occur will be considered, not just maximal ones. For example, a four-level RTS can have three to six different amplitudes, because the ones which do not occur during measurement are not taken into account.

Bi-level RTS centers will be defined as independent centers, each of them leading to only two levels, whereas a multi-level source will be a center which can generate several levels.

B. Detection method and improvements

A RTS detection and analysis tool based on an edge detection method has been proposed in [8]. It has become the basis of most DC-RTS studies in solid state image sensors and detectors [8]–[13] , and proved to be reliable and robust. This method also permitted to discriminate total ionizing dose and displacement damage dose contributions in DC-RTS [14] and allowed to develop an empirical prediction model for amplitudes of transition [15], [16].

Fig. 2 shows the new parameters extraction capabilities added to this tool. Post processing methods have been improved, but the detection method has not changed from [8].

Thanks to this tool, one can easily obtain the number of RTS levels, the evolution of dark current in each detected pixel with time, and their template, that is to say the modeled RTS signal calculated from the experimental data (some typical signals are given in Sec. III-A). In this work, 50 000 images and 50 step filter coefficients have been chosen. Once RTS pixels have been detected, post processing is used to determine statistical characteristics. Some usual notions have been extended for multi-level RTS, such as for time constants and amplitudes. As in previous work [8], the plot of the histograms of number of levels, amplitudes and times

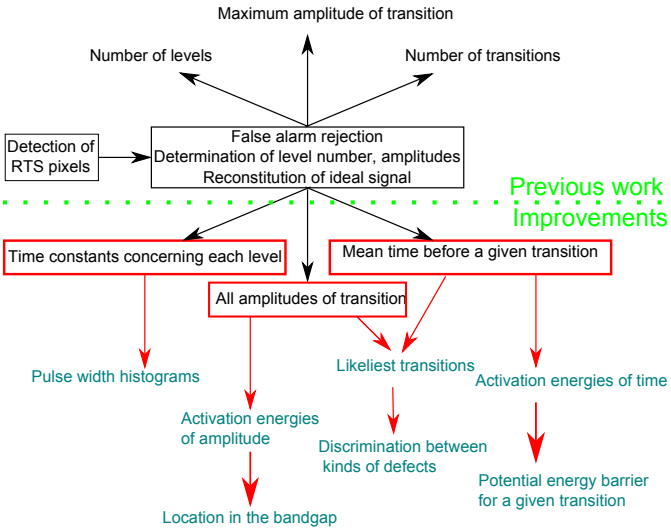

Fig. 2. Schematic of previous algorithm and its improvements.

is still possible. But some improvements have been made in order to adapt to multi-level RTS:

- all amplitudes (between couples of levels) which occur are considered
- all average times per level and time constants of RTS pixels can be calculated
- histogram of pulse widths can be plotted
- activation energies can be extracted from amplitudes and time constants, giving respectively some information about the centers location in the bandgap and their stability in a given configuration

III. Experimental Results

The measurements were conducted with a 512x512 4T-Pinned Photodiode CMOS image sensor with a pitch of 7 μm^3. It has a depleted volume of about 30 μm^3, and is fabricated in a commercially available 0.18 μm process. The CIS was irradiated grounded at Université Catholique de Louvain (UCL) facility with 22 MeV neutrons beam for a total displacement dose of 400 TeV/g. Measurements were held six weeks after irradiation. Processing was performed thanks to 50 000 images acquired with an integration time of 0.5 s, for 6 different temperatures (from 2°C to 22°C).

A. Different kinds of RTS centers

A RTS exhibiting more than two levels may come from a multi-level source, several independent bi-level centers or a combination of both. Consequently, the discrimination between these two kinds of centers could be useful to characterize them.

It is assumed that the probability to have two independent bi-level RTS with the same amplitude in the same pixel is very low: this implies that a three-level RTS is necessarily due to multi-level centers. It is also admitted that the probability for two centers to switch simultaneously is unlikely: it implies that if a four-level RTS is due to two independent

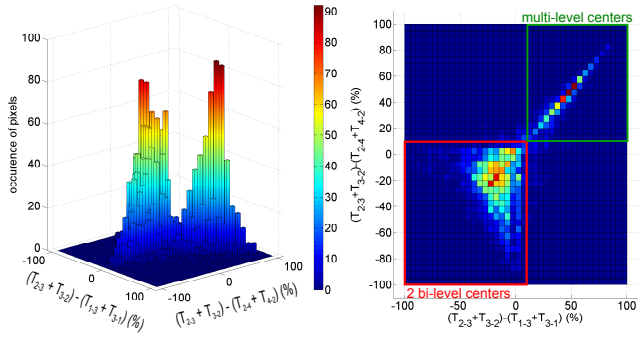

Fig. 3. Difference between number of transitions for four level RTS pixels. Values belong axis x and y are given in percentage (i.e divided by the number of transitions and multiplied by 100). Two groups can be separated.

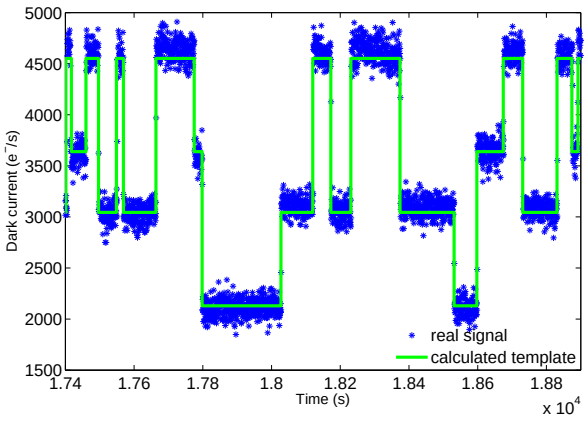

Fig. 4. Temporal evolution of two independent bi-level centers. The transition between the second and third level never occurs.

bi-levels, the transition between the second (low-middle) and third (middle-high) level would never occur. Thus, two kinds of four-level RTS stand out: four-level due to two different bi-level centers, and four-level RTS due to a single multi-level center (see for example Sec. III-A).

The criterion that will be used to automatically distinguish these two kinds of centers, is the fact that the transitions between the second and the third level is really rare (rarer than transitions between the first and third level and between the second and fourth level). Fig. 3 represents the difference between the number of transitions T_{2-3}(back and forth) and the number of transitions T_{1-3} or T_{2-4} (back and forth too) in terms of percentage for four level RTS pixels. It shows that two populations can be extracted, and an optimal threshold can be used to separate the two populations. There, a four-level RTS pixel is considered as two bi-levels RTS if

$T_{1-3} + T_{1-3} > 0.9 \times (T_{2-3} + T_{2-3})$ and

$T_{2-4} + T_{4-2} > 0.9 \times (T_{2-3} + T_{2-3})$.

What is also noticeable about the discrimination, is that for four-level caused by two different bi-level centers, the same amplitudes are discovered from the first to the second level and from the third and fourth level, which is expected because it is due to the same center. A similar method can be held about the amplitudes from the first to the third level and from the second and fourth level. This assessment is shown in Sec. III-C1, where it is observed that the curves plotted for the same centers (amplitudes 1-2 and 3-4, 1-3 and 2-4) are superimposed. This confirms that the criterion chosen looks appropriate.

Considering four-level RTS due to two bi-level centers at 2°C, the likeliest transitions between two levels can be investigated. Tab. I shows this analysis, and represents the mean probabilities of transition on 3195 four-level RTS pixels due to two bi-level centers. The expected possible transitions are very more likely (about 50 times) than the others.

Consequently, it is possible to separate the two signals coming from both centers, and to extract their own amplitude and time constants as represented on Fig. 5.

TABLE I

MEAN LIKELIEST TRANSITIONS OF FOUR-LEVEL RTS DUE TO TWO BI-LEVEL CENTERS. COLUMNS REPRESENT THE STATE BEFORE THE TRANSITION, AND ROWS REPRESENT THE STATE AFTER THE TRANSITION. THE VALUE OF EACH CELL GIVES THE PROBABILITY FOR A GIVEN TRANSITION TO OCCUR.

		level before transition			
		low (1)	low-middle (2)	middle-high (3)	high (4)
level after transition	low (1)	0	12.1 %	10.2 %	0.4 %
	low-middle (2)	12.0 %	0	0.9 %	11.3 %
	middle-high (3)	10.3 %	0.9 %	0	15.0 %
	high (4)	0.4 %	11.2 %	15.2 %	0

Moreover, considering four-level RTS due to a multi-level center at 2°C, the likeliest transitions can be investigated. Tab. II shows this analysis and represents the mean probabilities of transition on 1845 four-level RTS pixels due to multi-level centers.

It shows that the transitions which occur frequently are these from one level to the one just above or just below (some examples of temporal evolution are given in

TABLE II

MEAN LIKELIEST TRANSITIONS OF FOUR-LEVEL RTS DUE TO MULTI-LEVEL CENTERS. COLUMNS REPRESENT THE STATE BEFORE THE TRANSITION, AND ROWS REPRESENT THE STATE AFTER THE TRANSITION. THE VALUE OF EACH CELL GIVES THE PROBABILITY FOR A GIVEN TRANSITION TO OCCUR.

		level before transition			
		low (1)	low-middle (2)	middle-high (3)	high (4)
level after transition	low (1)	0	13.0 %	2.8 %	0.3 %
	low-middle (2)	13.0 %	0	15.6 %	3.2 %
	middle-high (3)	2.8 %	15.6 %	0	15.1 %
	high (4)	0.3 %	3.2 %	15.1 %	0

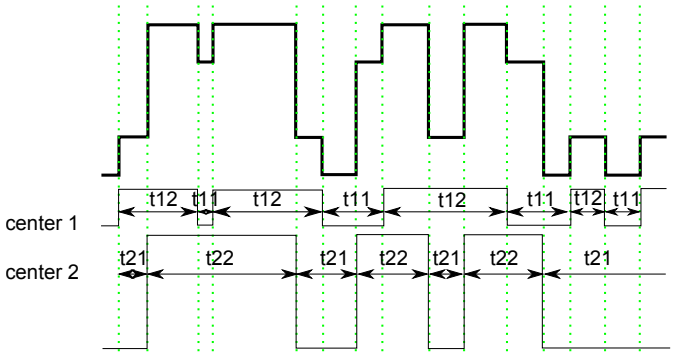

Fig. 5. Extraction of the influence of both centers. They can be considered independently and have their own amplitude and time constants. t11 and t12 represent the times spent in the first or second configuration for the first center, and respectively, t21 and t22 represent the times spent in the first or second configuration for the second center.

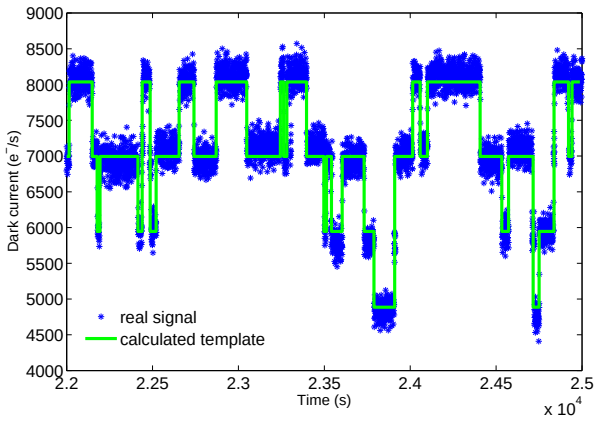

Fig. 6. Temporal evolution of a multi-level source. The transition between the second and third level often occurs.

Sec. III-C2 and demonstrates that this trend affects most of four-level RTS due to a multi-level center). Thus the easiest jump in dark current appears to be the jump to the state just around, but this is not necessarily the easiest jump in potential energy. Indeed, the levels are not necessarily correlated to the defects potential energy. This assumption is demonstrated below in Sec. III-C2 where some configuration coordinate diagrams are defined and presented. In what follows, only transitions from one level to an adjacent level will be considered for multi-level centers.

B. Study at 22°C

1) Amplitudes of RTS pixels: In order to be able to study multi-level RTS more in details, all transitions which occur have to be considered. Indeed, the possibility to access all amplitudes can provide more information about RTS centers generation rates. If two different amplitudes happen in the signal of the same pixel, it could reflect the contribution of several centers. That is why in Fig. 7, the histogram of all amplitudes is plotted, as well as the one of maximum amplitudes which is often shown in the literature. As previous work [3], the empirical prediction model described in [8] is

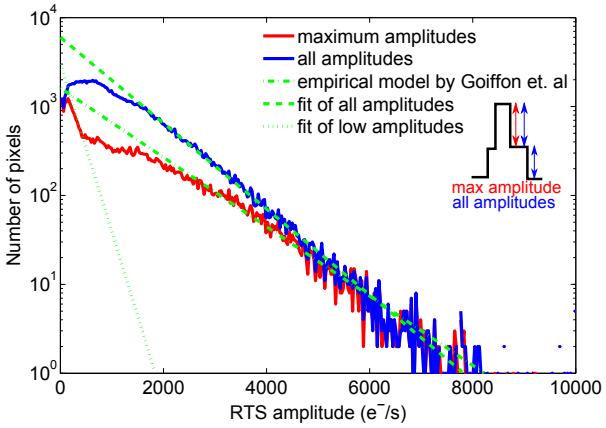

Fig. 7. Histogram of RTS amplitudes. The empirical prediction model shows an exponential mean of 1110 e⁻/s at 22°C.

still valid for maximum amplitudes (with a mean of 1200 e⁻/s at 23°C, that is to say 1110 e⁻/s at 22°C) and fits well, but not for all amplitudes. Nevertheless, an exponential shape is still noticeable for the histogram of all amplitudes with a mean amplitude of about 900 e⁻/s. This is slightly lower than for maximum amplitudes because lower amplitudes are taken into account.

The exponential mean of 220 e-/s at low amplitudes on the left side has typically been reported [3], [14], [16] for oxide RTS centers. However, at this given neutron fluence, the deposited TID is about 5 rad [17]. The expected density of TID induced RTS [16] at this level is about 8600 pixels (here there are about 12700 pixels), which is lower than the population in this peak. Moreover, if a significant TID induced RTS contribution was present, the number of RTS pixels would rise significantly when the TG is placed into depletion during integration. This particular measurement has been performed and the number of additional RTS pixels was not significant. Hence, it can be concluded that, despite an amplitude distribution that looks similar to TID induced RTS, this peak is coming from another source induced by displacement damage. One possibility would be a contribution from RTS centers outside the depletion region that would generate an RTS dark signal through a diffusion mechanism. To verify this hypothesis, activation energy measurements were performed on a limited temperature range (17°C-22°C) on this particular population and a value of 0.8 $\pm$ 0.3 eV was found, which is compatible with a diffusion driven transport. Such diffusion DC-RTS has never been reported before probably because neutron irradiation induced RTS in PPD-CIS has not been much studied in literature. More work is needed to confirm this hypothesis.

2) Pulse widths: In the literature, as in [1] [4], it is concluded that the two histograms of pulse widths of a two-level RTS (that is to say the histograms of times spent in a given level between two transitions) follow an exponential process, but this assessment has never been checked on

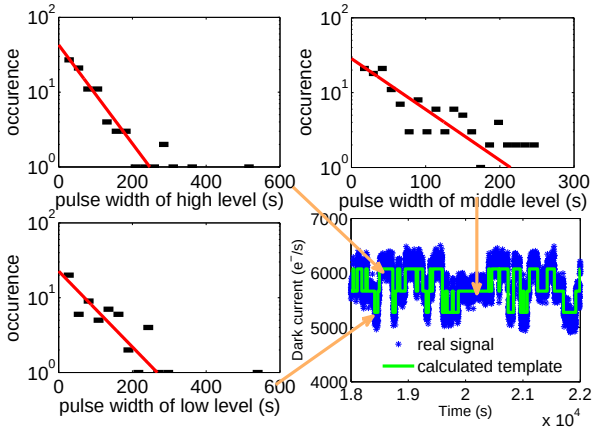

Fig. 8. Histograms of pulse widths for a given pixel with three levels. At 22°C, the mean time constants are 86 s in the low level, 64 s in the middle level, 66 s in the high level. The uncertainty is about 20s with this dataset.

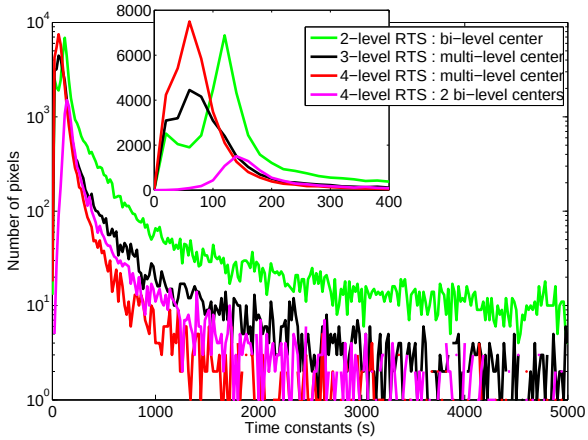

Fig. 9. Histograms of time constants. Mean times before a given transition are used, and for the last curve, the influence of both center has been separated to well consider the two centers time constants.

multi-level RTS.

In Fig. 8, considering the signal of a typical three-level RTS pixel, the three distributions of pulse widths about each level are plotted (a part of the the pixel dark signal evolution with time is also represented). As expected for Poisson processes, the histograms have an exponential behavior, which allows to extract new average times in each level thanks to the exponential fit.The found values are 86 s in the low level, 64 s in the middle level, 66 s in the high level. It can be concluded that this multi-level RTS is a Poisson process as two-level RTS and this is also confirmed on the whole multi-level RTS population with enough transitions.

3) Time constants: Fig. 9 represents time constants histograms. For 2-level RTS, many pixels have a transition rate of 150 s, represented by the green peak. For multi-level centers (black and blue curves), the time constants are lower, indicating that multi-level centers seem to be less stable in their configurations, and switch more frequently. As for four-level RTS which are the combination of two bi-levels centers, the peak is also around 150 s, as well as for 2-levels RTS. For bi-level centers, down and up time constants are quite different (see for example Sec. III-C2) but their average value is up to 120 s at 22°C whereas for multi-level centers, the average of each time constant is around 70 s. Concerning the global shape, all curves seem to have an 1/(time constant) shape (here $\frac{2.10^6}{|time\ constant-110|^{1.5}}$ is found for the curve of 2-level RTS).

C. Temperature behavior

The behavior of RTS characteristics with temperature is often observed [1], [3], [4], [6], [9], [10] to extract activation energies. Table. III shows some results which were previously found.

However, these values concern bi-level RTS pixels, and do not consider the complexity of multi-level centers. The following paragraphs show activation energies of amplitudes and time constants found during this study, for 2-level RTS as well as for multi-level centers.

TABLE III
ACTIVATION ENERGIES FOUND IN THE LITERATURE.

	Irradiation	activation energy (eV)
[1]	proton	amplitude : 0.57 ± 0.03 down time : 0.89 ± 0.1 up time : 0.87 ± 0.07
[3]	neutron	amplitude : 0.58
[4]	proton	down time : 0.58 up time : 0.61
[6] on DRAM	no irradiation	down time : 0.87 up time : 1.02
[9]	proton	low amplitude : 0.69 ± 0.02 high amplitude : 0.48 ± 0.03
[10]	proton	amplitude : 0.75

1) Amplitudes: The behavior of RTS amplitudes with temperature follows an Arrhenius law given by:

$$A \propto \exp\left(\frac{-E_a}{kT}\right) \quad (1)$$

Thus, the slope of the semi logarithmic plot provides the activation energy of the center, which is linked to its energy level in the bandgap. For 2-level RTS it has been widely studied, and some found values are given in table. III. They are mostly around the mid-gap signature.

Fig. 10 represents the mean amplitude of multi-level centers of 4 levels according to temperature. Only pixels detected as 4-level centers due to one single multi-level center on the whole temperature range are taken into account (here there are 72 pixels). The 3 extracted activation energies are 0.53 ± 0.11 eV for the amplitude from the first to second level, 0.53 ± 0.12 eV from the second to third level, and 0.52 ± 0.13 eV from the third to fourth level. The three activation energies are quite similar. The goodness of fit are respectively 0.9996, 0.9995, 0.9999.

Fig. 11 represents the mean amplitude of 4-level centers considered as the combination of two bi-level RTS according to temperature. Only pixels detected as 4-level centers due to two bi-level centers on the whole temperature range are

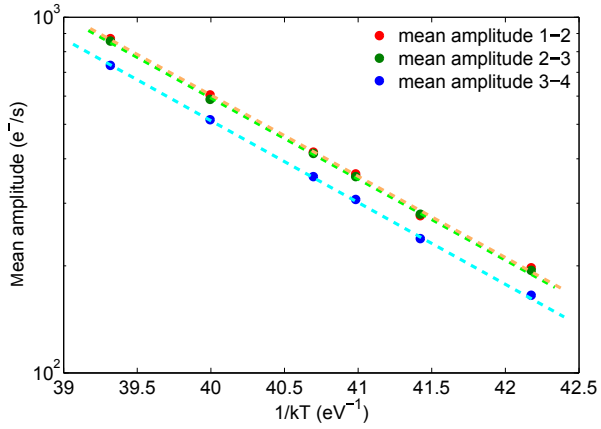

Fig. 10. Mean amplitude behavior with temperature for 4 levels RTS considered as multi-level centers. Levels are numbered from 1(low level) to 4(high level).

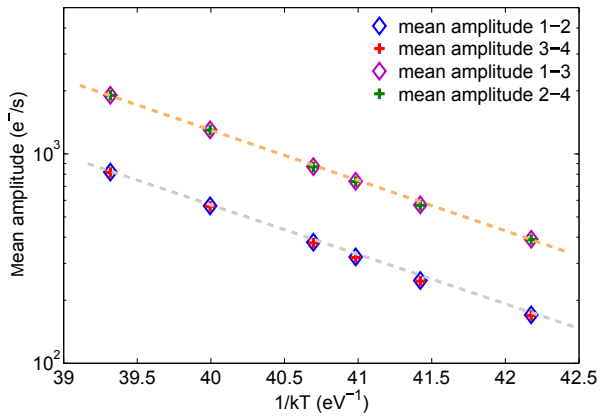

Fig. 11. Mean amplitude behavior with temperature for 4 levels RTS considered as 2 bi-levels. Levels are numbered from 1(low level) to 4(high level).

taken into account (here there are 603 pixels). Because there is one amplitude represented twice for each bi-level center, 4 amplitude activation energies are extracted.The values are 0.56 ± 0.07 eV and 0.56 ± 0.07 eV for the first defect, and 0.57 ± 0.05 eV and 0.57 ± 0.05 eV for the second defect. Each time, the goodness of fit is 0.9998. Fortunately, activation energies are equal for the contribution of the same center. The values are similar to the one found for 2-level RTS (0.57 eV). The centers appear to be located not far from the mid-gap of Silicon.

The mean activation energies for bi-level and multi-level centers seem to be slightly different, with a variation of 0.04 eV.

Fig. 12 represents the activation energy of amplitudes behavior with RTS amplitudes for 2-level centers. Most of activation energies are well distributed not far from 0.6 eV.

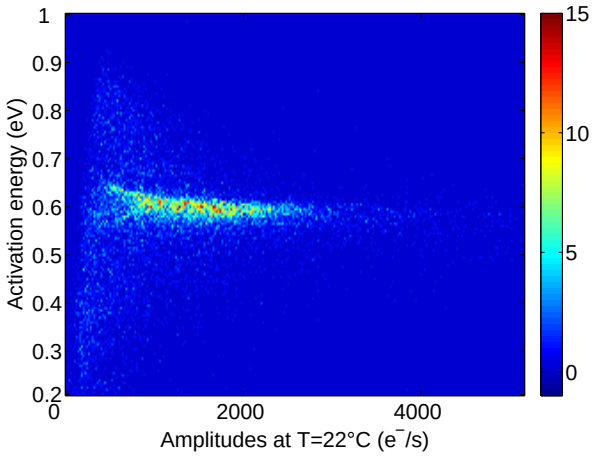

Fig. 12. Activation energy behavior with RTS amplitudes for 2-level centers.

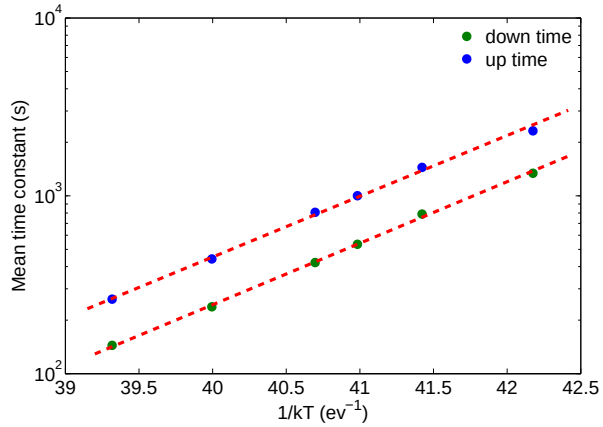

Fig. 13. Mean time constants behavior with temperature for 2-level centers.

2) Time constants: The behavior of RTS time constants τ with temperature follows an Arrhenius law, given by:

$$\tau \propto \exp\left(\frac{\mathrm{E_{time}}}{\mathrm{kT}}\right) \tag{2}$$

Indeed, as temperature increases, RTS signals switch more rapidly.Thus the slope of the semi-logarithmic plot permits to access activation energies E_{time}, which means the potential energy barriers to go from a configuration to another. Fig. 13 represents the mean time constants of 2-level centers. Only pixels detected as 2-level RTS at each temperature are taken into account (here there are 10152 pixels). The extracted activation energies are 0.77 eV for the down time and 0.72 eV for the up time. The goodness of fit are respectively 0.9984, 0.9962. As these time constants activation energies correspond to the barrier heights in potential energy to go from a configuration to another, a diagram representing these barriers can be drawn to illustrate the easiest jumps (see also [1] [18]). Hence, this diagram, called "'configuration coordinate diagram"'given in Fig. 14, shows the two potential wells for the two distinct RTS levels. As previous work [1],

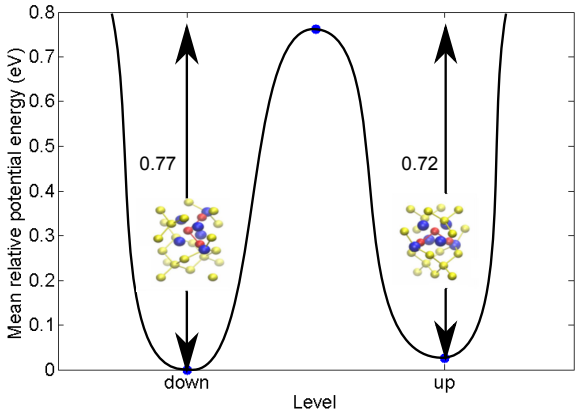

Fig. 14. Configuration diagram for 2-level centers. Two possible configurations of the center are illustrated [18] .

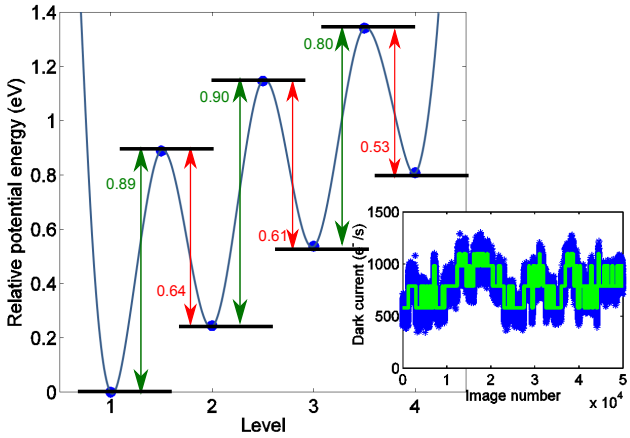

Fig. 15. Configuration diagram for a 4-level center considered as a multi-level center. Levels are numbered from 1(low level) to 4(high level).The temporal evolution of the dark current at 2°C is also shown.

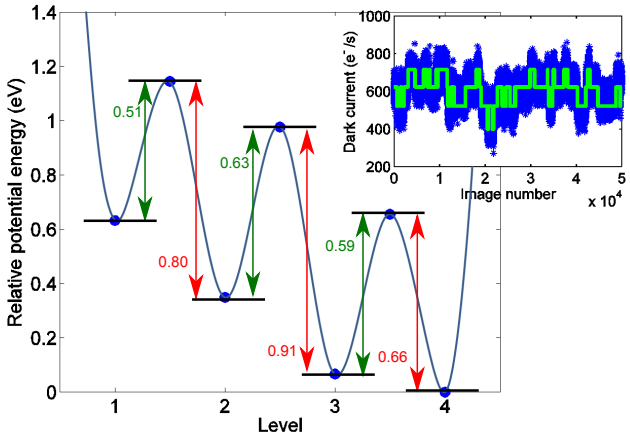

Fig. 16. Configuration diagram for a 4-level center considered as a multi-level center.Levels are numbered from 1(low level) to 4(high level).The temporal evolution of the dark current at 2°C is also shown.

similarities between up and down times activation energies have been found, even if the time constants ratio is about 2 for each temperature.

Concerning four-level RTS due to a multi-level center, the notion of configuration diagram can be extended. As it is considered that likeliest transitions are from one level to an adjacent, only neighbor transitions are taken into account. That is why a 2D plot is sufficient. According to the barriers height, there are 24 possible trends of configuration diagrams. Figs. 15, 16 and 17 show three distinct trends for several multi-level centers of four levels. The shape of the configuration diagram illustrated in Fig. 15 is found for 22% of four-level RTS pixels due to a single multi-level center, and shows that the dark current increases (level 1 corresponds to the low level which has the lowest generation rate, and level 4 corresponds to the high level which has the highest generation rate) as the relative potential energy increases too. But this is not always the case, as it can be observed in Fig. 16 (this configuration diagram is observed in 6% of cases) and Fig. 17 (this configuration diagram is observed in 8% of cases).Hence, it appears that potential energies and dark current levels are not correlated.

Thus, it seems to be difficult to build one mean configuration diagram for all multi-level centers.

IV. Discussion

Experimental results show that two kinds of centers can be discriminated. They do not have the same characteristics, as shown in Table. IV.

The mean amplitudes for multi-centers seem to be slightly lower than for bi-level centers. It could be consistent with the fact that they are slightly further from the mid-gap value and thus they generate fewer charges. Moreover, the fact that activation energies for amplitudes are less than the mid gap value (0.63 eV), can infer three possibilities :

- electric field enhancement, but it seems to be unlikely because at high amplitudes, the activation energies do not fall, as shown in Fig. 12
- bandgap narrowing [19]
- inter-center charge transfer [20]

Some ab-initio simulations [18], which consist in calculating and evaluating energy-levels in the bandgap, will be held to try to understand the phenomenon.

The multi-level centers change in configurations appears more often than for bi-level centers, which means that they could be less stable. But bi-level and multi-level centers time constants activation energies are widely spread, and it seems difficult to conclude if one kind would have lower or higher potential energy barriers.

Finally, configuration diagrams for multi-level RTS centers can exhibit distinct forms. For those which have four levels coming from a single multi-level center, 24 configurations are possible. Among these configurations, one is more represented (in 22% of cases) than others. Thus, it could be inferred that the configurations in Fig. 16 and Fig. 17, the likeliest transition is not from one level to the adjacent one,

TABLE IV
SUM-UP OF MAIN CHARACTERISTICS. LEVELS ARE NUMBERED FROM 1(LOW LEVEL) TO 4(HIGH LEVEL). τ_{x-y} MEANS MEAN TIME IN LEVEL X BEFORE GOING TO LEVEL Y.

	2-level RTS	3-level RTS	4-level RTS	
	bi-level center	multi-level center	2 bi-level centers	multi-level center
number of pixels	10152	414	72	603
mean amplitude at 22°C	1230 (e^-/s)	975 and 910 (e^-/s)	1200 (e^-/s)	970, 860 and 730 (e^-/s)
mean amplitude activation energy	0.57 ± 0.1 eV	0.54 ± 0.2 eV	0.56 ± 0.07 eV	0.53 ± 0.1 eV
mean time constants at 22°C	up : 260 s down : 145 s	up : 85 s middle : 90 s down : 75 s	up : 260 s down : 157 s	up : 52 s middle_up : 63 s middle_down : 60 s down : 50 s
mean potential energy barrier	up : 0.77 ± 0.4 eV down : 0.72 ± 0.4 eV	τ_{3-2} : 0.72 ± 0.4 eV τ_{2-3} : 0.70 ± 0.4 eV τ_{2-1} : 0.68 ± 0.4 eV τ_{1-2} : 0.74 ± 0.4 eV	up : 0.82 ± 0.4 eV down : 0.75 ± 0.4 eV	τ_{4-3} : 0.63 ± 0.3 eV τ_{3-4} : 0.72 ± 0.5 eV τ_{3-2} : 0.70 ± 0.3 eV τ_{2-3} : 0.77 ± 0.3 eV τ_{2-1} : 0.73 ± 0.4 eV τ_{1-2} : 0.79 ± 0.4 eV

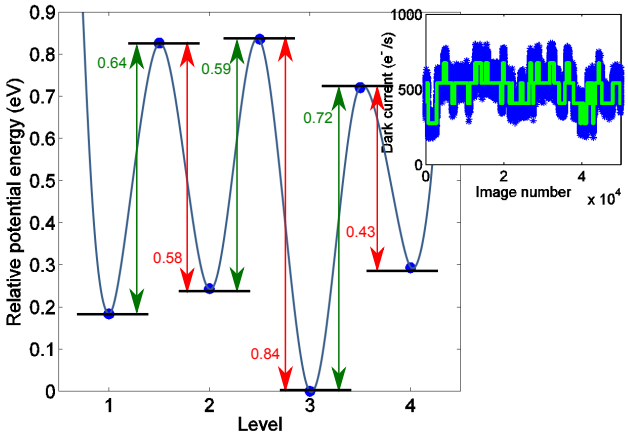

Fig. 17. Configuration diagram for a 4-level center considered as a multi-level center. Levels are numbered from 1(low level) to 4(high level).The temporal evolution of the dark current at 2°C is also shown.

but one can see in the temporal evolutions at 2°C that this in not the case. As a typical shape of configuration coordinate diagram cannot be obtained, one can deduce that there is no correlation between the level of dark current and the relative potential energy.

V. CONCLUSION

In this work, some post-processing improvements leading to new RTS analysis have been proposed. The definition of time constants for multi-level RTS has been clarified and distribution of all RTS amplitudes can be plotted. Moreover, the discrimination between bi-level centers and multi-level centers have been demonstrated thanks to the analysis of unlikeliest transitions. All these new possibilities permit to access to some information about the location of RTS centers states in the bandgap of Silicon through activation energies of amplitudes, and to the experimental defect relative potential energy through activation energies of times constants. It has finally been shown that for multi-level centers, the low level in dark current does not correspond necessarily to the level with the lowest potential energy.

ACKNOWLEDGMENT

The authors would like to thank the ISAE Image Sensor Team for their help, especially Romain Molina for the design of the image sensor, Jean-Baptiste Lincelles and Alice Pelamatti for their help in the data analysis. They would also like to thank Françoise Bezerra, CNES, and UCL (Université Catholique de Louvain) for the irradiation opportunities and facilities.

REFERENCES

[1] I. Hopkins and G. Hopkinson, "Random telegraph signals from proton-irradiated CCDs," *IEEE Trans. Nucl. Sci.*, vol. 40, no. 6, pp. 1567–1574, Dec. 1993.

[2] ——, "Further measurements of random telegraph signals in proton irradiated CCDs," *IEEE Trans. Nucl. Sci.*, vol. 42, no. 6, pp. 2074–2081, Dec. 1995.

[3] C. Virmontois, V. Goiffon, P. Magnan, S. Girard, C. Inguimbert, S. Petit, G. Rolland, and O. Saint-Pé, "Displacement damage effects due to neutron and proton irradiations on CMOS image sensors manufactured in deep submicron technology," *IEEE Trans. Nucl. Sci.*, vol. 57, no. 6, pp. 3101–3108, Dec. 2010.

[4] J. Bogaerts, B. Dierickx, and R. Mertens, "Random telegraph signals in a radiation-hardened CMOS active pixel sensor," *IEEE Trans. Nucl. Sci.*, vol. 49, no. 1, pp. 249–257, Feb. 2002.

[5] K. Abe, T. Fujisawa, H. Suzuki, S. Watabe, R. Kuroda, S. Sugawa, A. Teramoto, and T. Ohmi, "Statistical evaluation of dynamic junction leakage current fluctuation using a simple arrayed capacitors circuit," in *Reliability Physics Symposium (IRPS), 2010 IEEE International*, May 2010, pp. 683–688.

[6] P. Restle, J. Park, and B. Lloyd, "DRAM variable retention time," in *Electron Devices Meeting, 1992. IEDM'92. Technical Digest., International*. IEEE, 1992, pp. 807–810.

[7] D. Pogany, A. Chantre, J. Chroboczek, and G. Ghibaudo, "Origin of large-amplitude random telegraph signal in silicon bipolar junction transistors after hot carrier degradation," *Appl. Phys.Lett.*, vol. 68, no. 4, pp. 541–543, Aug. 1996.

[8] V. Goiffon, G. R. Hopkinson, P. Magnan, F. Bernard, G. Rolland, and O. Saint-Pé, "Multilevel RTS in proton irradiated CMOS image sensors manufactured in a deep submicron technology," *IEEE Trans. Nucl. Sci.*, vol. 56, no. 4, pp. 2132–2141, Aug. 2009.

[9] M. S. Robbins and L. Gomez Rojas, "An assessment of the bias dependence of displacement damage effects and annealing in silicon charge coupled devices," *IEEE Trans. Nucl. Sci.*, vol. 60, no. 6, pp. 4332–4340, Aug. 2013.

[10] E. Martin, T. Nuns, C. Virmontois, J.-P. David, and O. Gilard, "Proton and-rays irradiation-induced dark current random telegraph signal in a 0.18-cmos image sensor," *IEEE Trans. Nucl. Sci.*, vol. 60, no. 4, pp. 2503–2510, Aug. 2013.

[11] C. Virmontois, A. Toulemont, G. Rolland, A. Materne, V. Lalucaa, V. Goiffon, C. Codreanu, C. Durnez, and A. Bardoux, "Radiation-induced dose and single event effects in digital CMOS image sensors," *IEEE Trans. Nucl. Sci.*, vol. 61, no. 6, pp. 3331–3340, Dec. 2014.

[12] G. Winstone, M. Soman, E. Allanwood, A. Holland, J. Gow, K. Stefanov, and M. Leese, "Proton-induced random telegraph signal in the CMOS imaging sensor for JANUS, the visible imaging telescope on JUICE," in *SPIE Optical Engineering+ Applications*. International Society for Optics and Photonics, 2015, pp. 96 020N–96 020N.

[13] R. Zheng, R. Zhao, Y. Ma, B. Li, X. Wei, J. Wang, W. Gao, T. Wei, D. Gao, and Y. Hu, "A real-time auto-detection method for random telegraph signal (RTS) noise detection in CMOS active pixel sensors," *Journal of Instrumentation*, vol. 10, no. 07, p. C07013, 2015.

[14] V. Goiffon, P. Magnan, P. Martin-Gonthier, C. Virmontois, and M. Gaillardin, "Evidence of a novel source of random telegraph signal in CMOS image sensors," *IEEE Electron Device Lett.*, vol. 32, no. 6, pp. 773–775, Jun. 2011.

[15] C. Virmontois, V. Goiffon, P. Magnan, O. Saint-Pé, S. Girard, S. Petit, G. Rolland, and A. Bardoux, "Total ionizing dose versus displacement damage dose induced dark current random telegraph signals in CMOS image sensors," *IEEE Trans. Nucl. Sci.*, vol. 58, no. 6, pp. 3085–3094, Dec. 2011.

[16] C. Virmontois, V. Goiffon, M. S. Robbins, L. Tauziède, H. Geoffray, M. Raine, S. Girard, O. Gilard, P. Magnan, and A. Bardoux, "Dark current random telegraph signals in solid-state image sensors," *IEEE Trans. Nucl. Sci.*, vol. 60, no. 6, pp. 4323–4331, Dec. 2013.

[17] A. Witteles, "Neutron radiation effects on MOS fets: Theory and experiment," *IEEE Trans. Nucl. Sci.*, vol. 15, no. 6, pp. 126–132, Nov. 1968.

[18] A. Jay, M. Raine, N. Richard, N. Mousseau, V. Goiffon, A. Hemeryck, and P. Magnan, "Simulation of single particle displacement damage in silicon part II: Generation and long-time relaxation of the damage structure," *IEEE Trans. Nucl. Sci.*, 2017.

[19] J. Slotboom and H. De Graaff, "Measurements of bandgap narrowing in si bipolar transistors," *Solid-State Electronics*, vol. 19, no. 10, pp. 857–862, 1976.

[20] S. Watts, J. Matheson, I. Hopkins-Bond, A. Holmes-Siedle, A. Mohammadzadeh, and R. Pace, "A new model for generation-recombination in silicon depletion regions after neutron irradiation," *IEEE Trans. Nucl. Sci.*, vol. 43, no. 6, pp. 2587–2594, Dec. 1996.